Experimental Demonstration of sub-THz Wireless Communications Using Multiplexing of Laguerre-Gaussian Beams When Varying Two Different Modal Indices

Amir Minoofar, Xinzhou Su, Huibin Zhou, Runzhou Zhang, Fatemeh Alishahi, Kaiheng Zou, Hao Song, Kai Pang, Shlomo Zach, Moshe Tur, Andreas F. Molisch, Hirofumi Sasaki, Doohwan Lee, and Alan E. Willner

***Abstract*— The ability to multiplex multiple structured beams for sub-terahertz (sub-THz) wireless communications has been recently explored. The spatial orthogonality of structured beams enables mode-division multiplexing (MDM). In an MDM system, multiple data-carrying beams are transmitted and received simultaneously through a single aperture pair with low inherent crosstalk. This can increase data capacity and spectral efficiency of the system. Here, we experimentally demonstrate multiplexing orthogonal sub-THz Laguerre-Gaussian ($LG_{\ell,p}$) beams when varying two different modal indices (i.e., both ℓ and p); this contrasts with prior reports when varying only one index (i.e., ℓ) and could potentially provide a larger set of channels and beams in an MDM system. In our demonstration, specially designed phase patterns are used: (1) at the transmitter, to convert two THz Gaussian beams to two different LG beams, each carrying an independent data channel; and (2) at the receiver, to separate and convert the LG beams back to Gaussian-like THz beams. An 8-Gbit/s quadrature-phase-shift-keying (QPSK) link containing two multiplexed LG modes over 40 cm is experimentally demonstrated. For the above link, three different LG modal sets are chosen (i.e., {$LG_{-2,0}$ and $LG_{1,1}$} or {$LG_{3,0}$ and $LG_{0,1}$} or {$LG_{2,1}$ and $LG_{0,1}$}). All channels are recovered with bit error rates (BERs) below the 7% forward error correction (FEC) limit. The experimental results indicate that: (a) higher-order LG modes experience more divergence, larger size, and lower conversion efficiency, contributing to higher power loss; and (b) the modal coupling and crosstalk for different LG modes is < -12 dB, which could be due to the transmitter/receiver misalignments as well as beam truncation by the limited-sized receiver aperture.**

***Index Terms*— terahertz communication, terahertz photonics, mode-division multiplexing (MDM), Laguerre-Gaussian modes.**

I. Introduction

Exploiting 0.1 to 1 terahertz (THz) carrier frequencies in wireless communications has gained interest due to the potential for providing more system spectrum and capacity than millimeter waves [1-4]. Moreover, when comparing to free-space optical communications, THz waves tend to be less affected by atmospheric turbulence and weather conditions due to lower interaction with matter [5-6]. Additionally, we note that photonic technologies can play an important role in THz communications since photonics can enable accurate generation and frequency tuning of THz signals by heterodyning two sources at different wavelengths [7-11].

As with many types of communication systems, there is a motivation to further increase the capacity of these THz communication links by using multiplexing, with one example being MDM [12-14]. In an MDM system, multiple THz beams, each carrying an independent data channel, are simultaneously transmitted in the same frequency band [15]. In a typical MDM system, each beam with a structured amplitude and phase profile has one of N orthogonal modes from a modal basis set [16-19]. This orthogonality enables the multiplexing, spatial co-propagation, and demultiplexing of each data channel independently with low inherent crosstalk [16-18]. Moreover, MDM can be compatible with and complement other multiplexing techniques, such as frequency- and polarization-division multiplexing (FDM and PDM) [20-23].

An example of an orthogonal modal basis set is LG. $LG_{\ell,p}$ modes are characterized by two spatial modal indices: (1) azimuthal (ℓ), which is the number of 2π phasefront changes that occur in a circle around the center, and (2) radial (p), which is related to the number of concentric intensity rings in the beam [24-25]. Previous reports have shown the generation and multiplexing of orbital angular momentum (OAM) modes (i.e., a subset of LG modes) for THz frequencies [26-30]. In these prior art systems, the multiplexed spatial modes are varied in a one dimensional (1D) (i.e., different ℓ values but the same $p = 0$ value). Therefore, it might be valuable to experimentally demonstrate the potential of using both modal indices (e.g.,

This work was support by Vannevar Bush Faculty Fellowship sponsored by the Basic Research Office of the Assistant Secretary of Defense (ASD) for Research and Engineering (R&E) and funded by the Office of Naval Research (ONR) (N00014-16-1-2813); Defense Security Cooperation Agency (DSCA) (4440646262); Airbus Institute for Engineering Research; Qualcomm Innovation Fellowship (QIF).

A. Minoofar, X. Su, H. Zhou, R. Zhang, F. Alishahi, K. Zou, H. Song, K. Pang, A. F. Molisch, and A. E. Willner are with Department of Electrical Engineering, University of Southern California, Los Angeles, CA 90089 USA (e-mail: minoofar@usc.edu).

S. Zach, and M. Tur are with School of Electrical Engineering, Tel Aviv University, Ramat Aviv 69978 Israel.

H. Sasaki, D. Lee are with NTT Network Innovation Laboratories, NTT Corporation, Yokosuka 239-0847, Japan.

varying both ℓ and p) for such THz MDM systems. Compared with MDM using 1D OAM modal basis set (i.e., varying only ℓ), using 2D LG modal basis set (i.e., varying both ℓ, p) can provide an additional degree of freedom for mode multiplexing. Thus, using a 2D set of modes rather than a 1D set of modes could potentially provide a larger set of channels and beams for such THz MDM systems [24-25].

In this paper, we experimentally demonstrate THz wireless communications by multiplexing two LG beams with two different modal indices (i.e., different ℓ and p). At the transmitter, an optical data signal and a continuous wave (CW) laser are mixed in a photodiode for the generation of THz Gaussian beams, and different phase patterns (PPs) convert these beams to higher-order LG beams for MDM [31]. At the receiver, we use corresponding down-conversion PPs to convert the LG modes back into a Gaussian-like beam for data recovery after 40-cm free-space propagation. We demonstrate 8-Gbit/s communications at 0.3 THz using two LG beams, each carrying a 2-Gbaud QPSK data signal. Different LG mode combinations (i.e., $\{LG_{-2,0}$ and $LG_{1,1}\}$ or $\{LG_{3,0}$ and $LG_{0,1}\}$ or $\{LG_{2,1}$ and $LG_{0,1}\}$) for multiplexing are explored. The results show that: (a) higher-order LG modes could experience more power loss (e.g., $LG_{2,1}$ has 4-dB higher power loss compared to $LG_{1,1}$), which might be due to the larger beam divergence and lower conversion efficiency for the LG beam generation; (b) the modal coupling and crosstalk among the two modal sets is < -12 dB, which could be due to link misalignment and beam truncation by the limited-sized receiver aperture; (c) BERs below the 7% FEC limit are achieved for all modal sets; (d) the multiplexed LG beams suffer a signal-to-noise ratio (SNR) penalty of ~1 dB.

II. Concept and Experimental Setup

A. Concept

Figure 1 illustrates the concept of using multiplexing of LG beams, in which both modal indices can be varied, for THz communications. First, two Gaussian modes, each of which carries an independent data stream, are generated at the transmitter. Then they pass through two different PPs for the generation of LG beams. These PPs are crafted such that the two output THz beams are orthogonal to each other and maintain their orthogonality in free-space propagation (in the absence of turbulence and other perturbations). The two LG beams are spatially combined and transmitted through a single aperture transmitter aperture. As can be seen in the 2D modal spectrum of the THz beams, each beam has different ℓ and p indices, which indicates the MDM is utilized in a 2D modal space. At the receiver, a beam splitter creates two copies of the multiplexed THz beams. Finally, after passing through the corresponding down-conversion PPs, the two LG modes are converted back into the fundamental Gaussian mode (i.e., $\ell = p = 0$) to enable data recovery by the THz receiver. In this paper, we demonstrate such an LG-based MDM THz system at a carrier frequency of 0.3 THz, which has gained much interest because of its low atmospheric losses [20].

B. Generation and down-conversion of LG modes

The concept of generating and down-converting THz LG modes is described in detail in Figs. 2(a, b). A blazed grating with a periodic phase along one axis and a specific diffraction angle can diffract an incident Gaussian beam to a tilted direction compared to its propagation axis, as shown in Fig. 2(a1). This diffraction angle corresponds to the grating period [32-35]. By manipulating the efficiency of the blazing pattern, the beam intensity can be attenuated at a specific point in a transverse plane. By tailoring the grating period, the beam redirects to

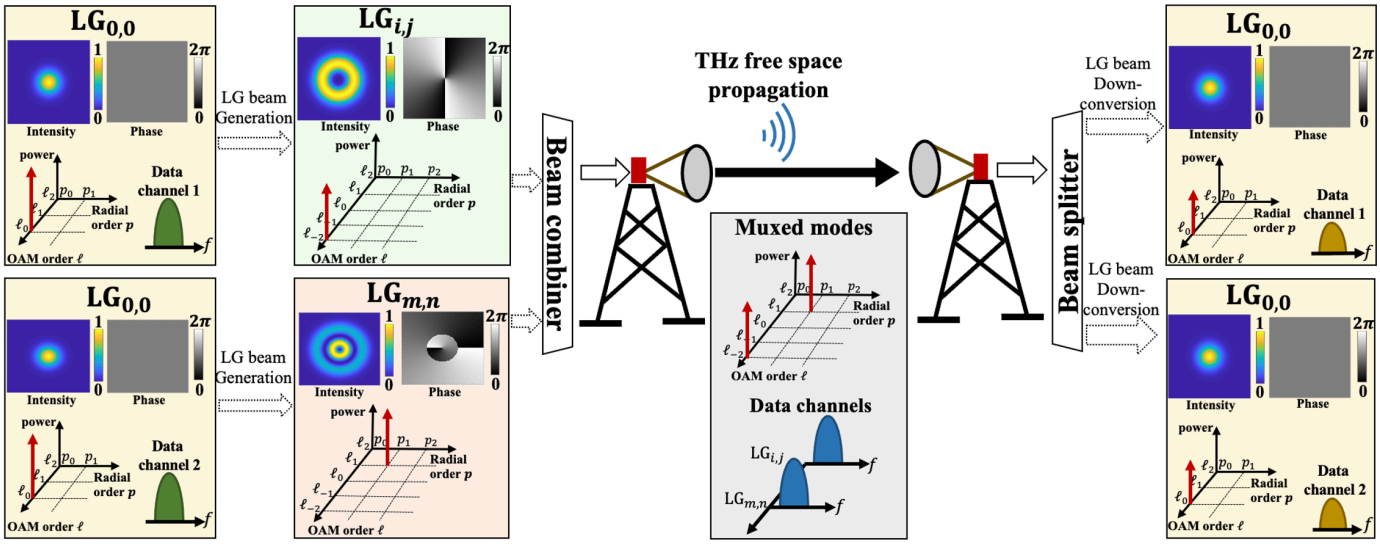

Fig. 1. Concept of the MDM of beams having two different LG modal indices. First, two THz Gaussian beams (i.e., $LG_{0,0}$) with the same frequency are passed through different phase patterns to generate two distinguished LG modes (i.e., $LG_{i,j}$ and $LG_{m,n}$). Second, these two LG modes are multiplexed and coaxially propagate through the free-space medium using a single aperture at the same frequency. Finally, to recover each of the modes, corresponding phase patterns are used to convert them back into the fundamental Gaussian mode, thereby enabling data recovery by the THz receiver.

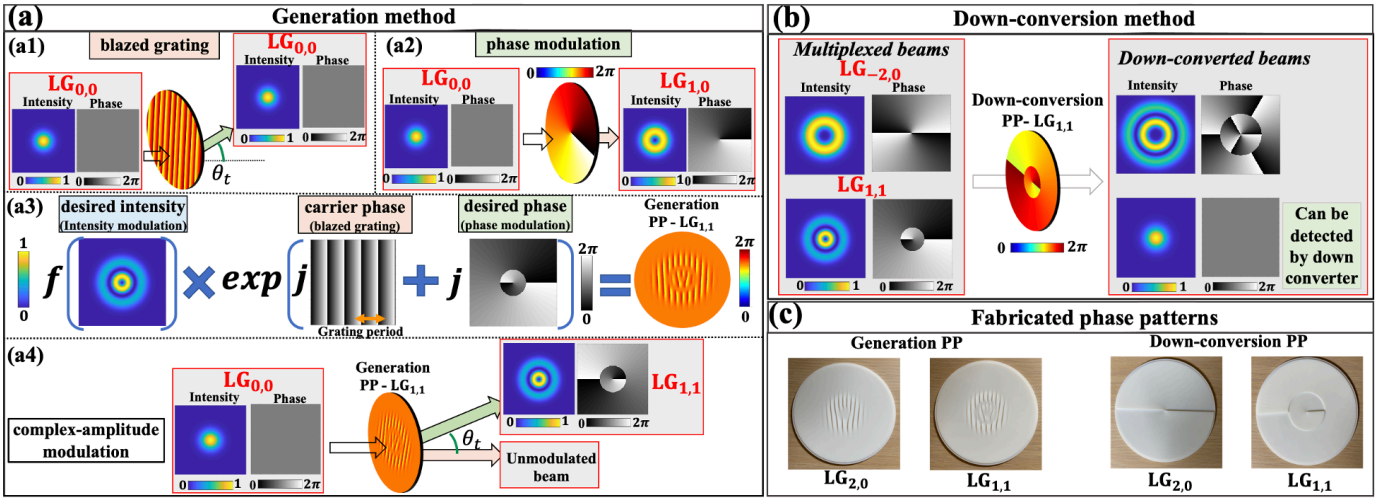

Fig. 2. (a) Generation approach for creating LG modes in the THz frequency range. (a1) A blazed diffraction grating diffracts an incident Gaussian beam to a tilted direction, which corresponds to the grating period. θ_t is the diffraction angle. (a2) A Gaussian beam is converted to an OAM mode by creating a helical phase front when passes through a spiral phase plate (SPP). (a3) For complex-amplitude modulation, both blazed grating and SPP are combined and multiplied by a function of the intensity of the desired LG mode as a mask to generate an LG mode. (a4) An incident Gaussian beam is converted to the desired LG mode at a specific diffraction angle by passing through the phase pattern. The unmodulated portion of the beam remains in the same axis. (b) A corresponding down-conversion phase pattern converts the LG beam, which matches with its phase profile, into the Gaussian-like beam to enable data recovery. (c) Photos of fabricated phase patterns with a 10 cm diameter for both generation and down-conversion and for $LG_{-2,0}$ and $LG_{1,1}$ modes.

different angles. For our case, the grating period is 4.5 mm on the horizontal axis, which diffracts the 0.3 THz beam by a ~13° diffraction angle. One straightforward way to generate a helically phased beam is to use spiral phase plates (SPPs) with a helical surface [16-17]. Due to its subsequent helical phase structure, the beam is spatially phase-modulated with a factor of exp $(j\ell\theta)$ in the azimuthal direction corresponding to its designed OAM order (ℓ), as shown in Fig. 2(a2).

To generate an LG mode with a high mode purity, a complex-amplitude modulation (i.e., modulating both phase and amplitude) is required. Using a phase-only element and combining a blazed diffraction grating and phase modulation, the phase and amplitude can be modulated jointly, thereby generating THz LG modes. In this method, a function of intensity of the desired LG mode is multiplied with the superposition of phases, including an SPP and a blazed grating [33-36], as depicted in Fig. 2(a3). This results in an amplitude modulation for the portion of the input Gaussian beam that will be diffracted by the blazed grating. Accordingly, at a sufficient distance from the PP and at a specific diffraction angle (e.g., 30 cm and 13° for our case, respectively), over which the unmodulated zeroth-order and modulated (i.e., LG mode) portions are separated, the desired LG mode is generated, as shown in Fig. 2(a4).

To down-convert the generated THz LG modes to Gaussian modes, a spatial phase modulation technique is used, as presented in Fig. 2(b). Subsequently, a properly designed PP down-converts a specific LG mode to a Gaussian-like mode for detection by the THz receiver. Note that the spatial phase modulation technique has higher conversion efficiency than that of the complex-amplitude modulation technique, but it also results in lower mode purity [24-25, 33]. We choose the spatial phase modulation rather than an inverse of complex-amplitude modulation because the former one alleviates the need for another separation distance and detection of angle on the receiver side.

Figure 2(c) shows the fabricated PPs that are used for generating and down-converting the $LG_{1,1}$ and $LG_{2,0}$ modes. The PPs have a diameter of 10 cm and are fabricated through a 3D printing process using a photosensitive resin material (i.e., VeroWhite glossy) with a refractive index of 1.655 at 0.3 THz. The amount of power absorption loss for a single blank PPs is ~ 4-dB, which is mainly due to the THz beam attenuation for the material of PPs. We believe that using diffractive optical elements having lower absorption loss at 0.3 THz, such as high-density polyethylene (HDPE) might help reduce the insertion loss [36].

C. *Experimental setup*

The experimental setup used in this study is depicted in Fig. 3. Figure 3(a) shows the generation, propagation, and detection of THz LG modes based on the photonic generation of THz signals. A 2-Gbaud QPSK data signal and a CW laser are combined and then divided into two copies. One of the copies is delayed from the other, thereby resulting in two decorrelated signals. The combined modulated signal and a CW laser are mixed in a positive-intrinsic-negative photodiode (PIN-PD) to generate 0.3 THz beams via the heterodyne photomixing. According to the stated approach shown in Fig. 2, the generated THz Gaussian beams are spatially modulated to generate two LG modes, which coaxially propagate to the receiver. Subsequently, the LG modes are converted back into the Gaussian-like beam for detection by the THz receiver.

The details of the experimental setup are illustrated in Fig. 3(b). Two tunable optical laser sources at $\lambda_1 = 1550.05$ nm and $\lambda_2 = 1552.45$ nm, in which $\Delta\lambda = \lambda_2 - \lambda_1$ corresponds to 0.3 THz as a carrier frequency, are used. An arbitrary waveform generator (AWG) drives the IQ modulator to modulate λ_1 with a Nyquist-shaped (roll-off factor of 0.1) 2-Gbaud QPSK data

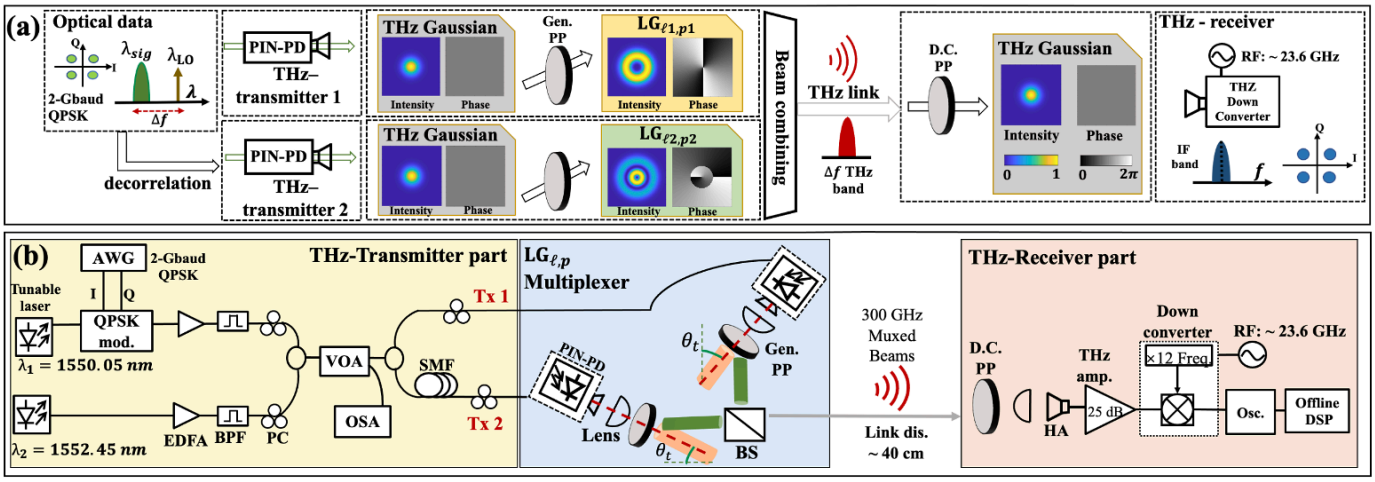

Fig. 3. (a) Concept of generation and detection of THz LG modes. A 2-Gbaud QPSK data signal and another CW laser are combined. The wavelength difference (i.e., $\lambda_{LO} - \lambda_{sig}$) corresponds to the 0.3 THz carrier frequency. The combined optical signal and a CW laser are split into two paths. One path is decorrelated, and both are fed into a PIN-PD to generate two Gaussian beams at 0.3 THz frequency. (b) Experimental setup. EDFAs, a VOA, and an OSA are used to amplify, adjust, and monitor, respectively, the input power of the PIN-PD. One lens for collimating and another for focusing the THz beams are used at the transmitter and receiver. These lenses have ~ 5 and ~ 10 cm focal lengths, respectively. After ~ 40 cm of free-space propagation, an HA with a 26-dB gain and a THz amplifier with a 25-dB gain are used to collect and amplify the received signal at the receiver side. Using an external RF source at 23.6-GHz, the received signal is down-converted to an IF band to be received by the oscilloscope for offline DSP and data recovery. PIN-PD: positive-intrinsic-negative photodiodes; PP: phase pattern; Gen. PP: generation PP; D. C. PP: down-conversion phase pattern; AWG: arbitrary waveform generator; EDFA: erbium-doped fiber amplifier; BPF: band pass filter; PC: polarization controller; VOA: variable optical attenuator; OSA: optical spectrum analyzer; SMF: single mode fiber; BS: beam splitter; HA: horn antenna; Osc: oscilloscope.

signal. The modulated light is subsequently amplified using an erbium-doped fiber amplifier (EDFA). Then, it is combined with λ_2 and equally split into two copies. A 15 m length single mode fiber (SMF) is used to impart delay on one copy and to create the second decorrelated data channel. We employ a variable optical attenuator (VOA) to adjust the input optical power to the PIN-PDs. Polarization controllers (PCs) are used to align the state of polarization of the optical signals launched into the PIN-PDs, which are polarization sensitive. In the case of the launched optical power being 30 mW and the reverse bias voltage being -1.5 V, the PIN-PDs have: (i) a 3-dB bandwidth of ~120 GHz, and (ii) a responsivity of 0.33 A/W [37-38]. At the transmitter, a lens with a ~ 5 cm diameter and 7.5 cm focal length collimates the THz beam before it passes through the generating PPs. At the receiver side, a lens with a ~10 cm diameter and 15 cm focal length focuses the THz beam. Subsequently, a diagonal horn antenna (HA) with a 26-dB gain and a low-noise THz amplifier with a 25-dB gain for frequencies between 0.26 and 0.33 THz are used to receive and amplify the THz data signal, respectively. A sub-harmonic mixer, which has a 40 GHz IF bandwidth and operates in the 0.22 to 0.33 THz band, is used to down-convert the received THz signal to an intermediate frequency (IF) signal. Another external radio frequency (RF) synthesizer of ~23.6 GHz is frequency multiplied by 12 and then used to drive the THz mixer to generate an IF at ~16.8 GHz. This IF corresponds to the following relationship: $f_{0.3\ \mathrm{THz}} = 12.f_{\mathrm{RF}} + f_{\mathrm{IF}}$. Finally, a digital oscilloscope captures the data streams, and the data are recovered using off-line digital signal processing (DSP).

D. Intensity profiles of THz LG modes

To characterize the generated THz LG modes, we obtain their intensity profiles both through simulation and experiment. Figure 4 shows the intensities of 0.3 THz LG modes, in which ℓ and p are {(0,0), (1,0), (2,0), (0,1), (3,0), (1,1), (2,1), and (1,2)}. For both simulation and experimental results, only the intensity of the spatially modulated beam (i.e., the desired LG mode) is measured. While the other unmodulated beam remains in the direction of the incident Gaussian beam and is not considered. Figure 4(a) presents the simulated intensities of LG beams at the link distance (i.e., ~ 40 cm from the generation PP). The simulation model has a pixel size of 1.5 mm and 500 × 500 pixels at the transverse plane. As can be seen from the intensity profiles, the number of rings equals $p + 1$. Here, the LG modes are sorted based on their order according to $|\ell| + 2p$ [39]. Additionally, the conversion efficiency is calculated by dividing the power of the final modulated beam into the total power of the incident beam to the generation PPs [40]. We can see that the conversion efficiency decreases with the order of LG modes (e.g., $LG_{1,2}$ beam has ~ 2.2-dB lower conversion efficiency compared to $LG_{1,1}$ beam).

To obtain these profiles through experiment, the sub-harmonic mixer is mounted on a 2D translation stage that can traverse the XZ axis with a resolution of 5 μm. The number of pixels is indicated for each profile in Fig. 4(b). The experimental results are similar to the simulation results. For both results, (i) the incident Gaussian beam (i.e., $LG_{0,0}$) has ~ 20 mm beam width, and (ii) after the PPs, different LG modes are generated with the designed beam width of ~ 10 mm. After propagation, the divergence of an LG mode scales with the mode order [41-43]. The table inside Fig. 4(b) shows the beam diameters of LG modes at 40 cm far from the generation PP. The beam width of each LG beam is measured by scanning its intensity profile. As can be seen, higher order LG modes have larger beam sizes due to the divergence corresponding to their

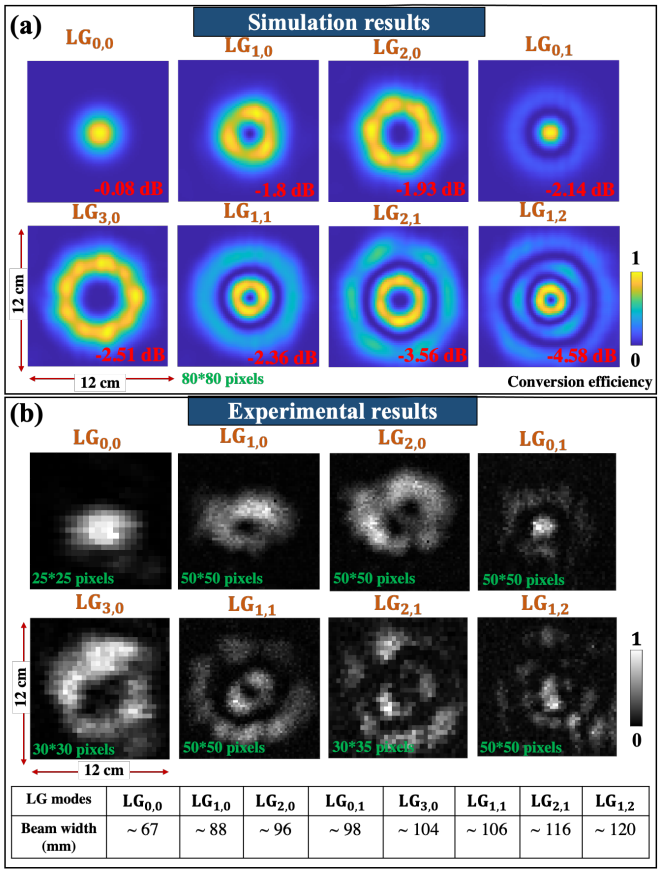

LG modes	$LG_{0,0}$	$LG_{1,0}$	$LG_{2,0}$	$LG_{0,1}$	$LG_{3,0}$	$LG_{1,1}$	$LG_{2,1}$	$LG_{1,2}$
Beam width (mm)	~ 67	~ 88	~ 96	~ 98	~ 104	~ 106	~ 116	~ 120

Fig. 4. (a) Simulation and (b) experimental results for the intensity of THz LG modes $(\ell, p) = \{(0,0), (1,0), (2,0), (0,1), (3,0), (1,1), (2,1), \text{and } (1,2)\}$. The table shows the beam width of different LG modes. For both the simulation and experiment: (1) the beam width of the Gaussian beam and LG beams are 20 mm and 10 mm, respectively; (2) the intensity of the generated beam is measured after 40 cm far from the generation phase pattern, when only considering the modulation portion of the resultant beam. In simulation, a pixel size of 1.5 mm and 500×500 pixels at the transverse plane are used.

mode orders. The results indicate that THz LG modes having higher modal indices (e.g., $LG_{1,2}$) experience higher power loss (e.g., $LG_{1,2}$ beam has ~ 4-dB lower power compared to $LG_{1,1}$ beam), which can be explained by: (a) the larger beam divergence [41-43] and (b) the decrease in the conversion efficiency for LG beam generation [32-33]. These effects make observing outer rings for these modes (e.g., $LG_{1,2}$) more difficult compared to lower-order modes (e.g., $LG_{1,1}$).

E. Interferograms of THz LG modes

The interferograms of THz LG modes are also measured to verify their characteristics. We use the interferometric arrangement to evaluate the interferograms of the LG modes experimentally, as shown in Fig. 5(a). A reference beam (i.e., $LG_{0,0}$) in the first branch and the generated LG beam at the second branch are combined in a beam splitter (BS). A 4-dB attenuator and a lens with a 75 mm focal length—both of which are 50 mm in diameter—are used to equalize the power and enlarge the beam size of the reference beam, respectively. Like intensity measurements, the sub-harmonic mixer, which is mounted on a 2D translation stage and is placed 60 cm far from the PP, is used to scan the received THz power.

The interferogram results when the modal indices of THz LG modes are varied among the set of $(\ell, p) = \{(0,1), (3,0), \text{and } (1,1)\}$ are shown in Fig. 5(a-b). To investigate the phase front, we first employ a simulation model with a pixel size of 1.5 mm and 500 × 500 pixels at the transverse plane. Then, a single Gaussian mode with 20 mm beam waist is interfered with the desired LG modes with 10 mm beam waist. Both the LG modes with $p \neq 0$ and OAM modes (i.e., $p = 0$) have a twisting shape that follows the OAM order (ℓ). However, another twisting pattern is observed for the $p \neq 0$ case at the outer rings due to the π phase difference between the two neighboring concentric rings [24-25]. The differences between the simulation and experimental results can be explained by: (a) some misalignment of the devices in the setup, (b) the lower resolution of experimental results compared to the simulation results, and (c) the fact that the emitted THz beam from the PIN-PD is not a pure Gaussian beam as shown in Fig. 4 (b).

It should be noted that we could get the mode purity of the generated LG modes using other approaches, such as off-axis digital holography [44]. Although, such approaches are not considered due to the limitation of experimental setup and explicitly the small diffraction angle of grating patterns (i.e., 13°). Furthermore, one can also measure the LG modal power spectrum and evaluate the power coupling to other LG modes, which requires fabricating multiple down-conversion PPs to find the optimum size for matching with the received beam size.

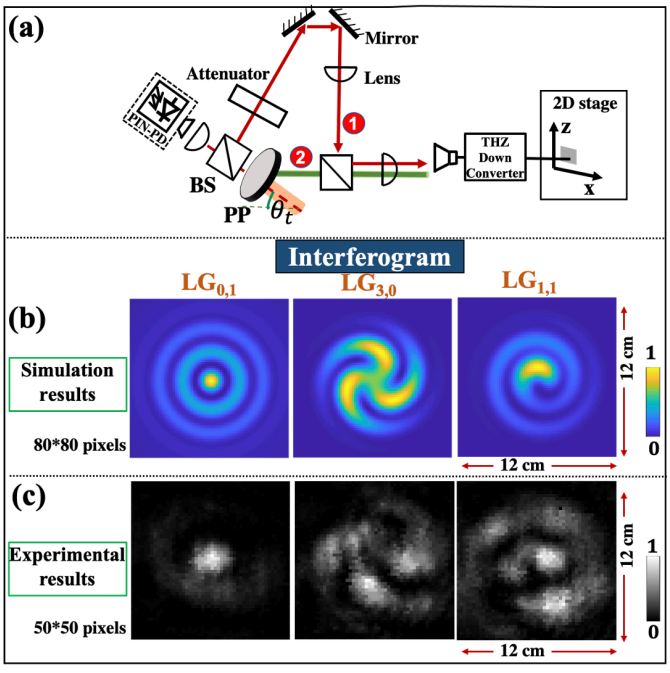

Fig. 5. (a) Experimental setup for capturing the interferogram images. An attenuator with 4 dB loss and a THz lens with 75 mm focal length both having 50 mm diameter are used to equalize the power of reference beam and generated beam as well as enlarge the reference beam, respectively. (b) Simulation and (c) experimental results for the interferograms of LG modes $(\ell, p) = \{(0,1), (3,0), \text{and } (1,1)\}$. A simulation model with a pixel size of 1.5 mm and 500×500 pixels at the transverse plane is used. The beam waist of Gaussian beam and LG beams are ~ 20 mm and 10 mm, respectively. The interferogram images are measured after 60 cm far from the generation PPs.

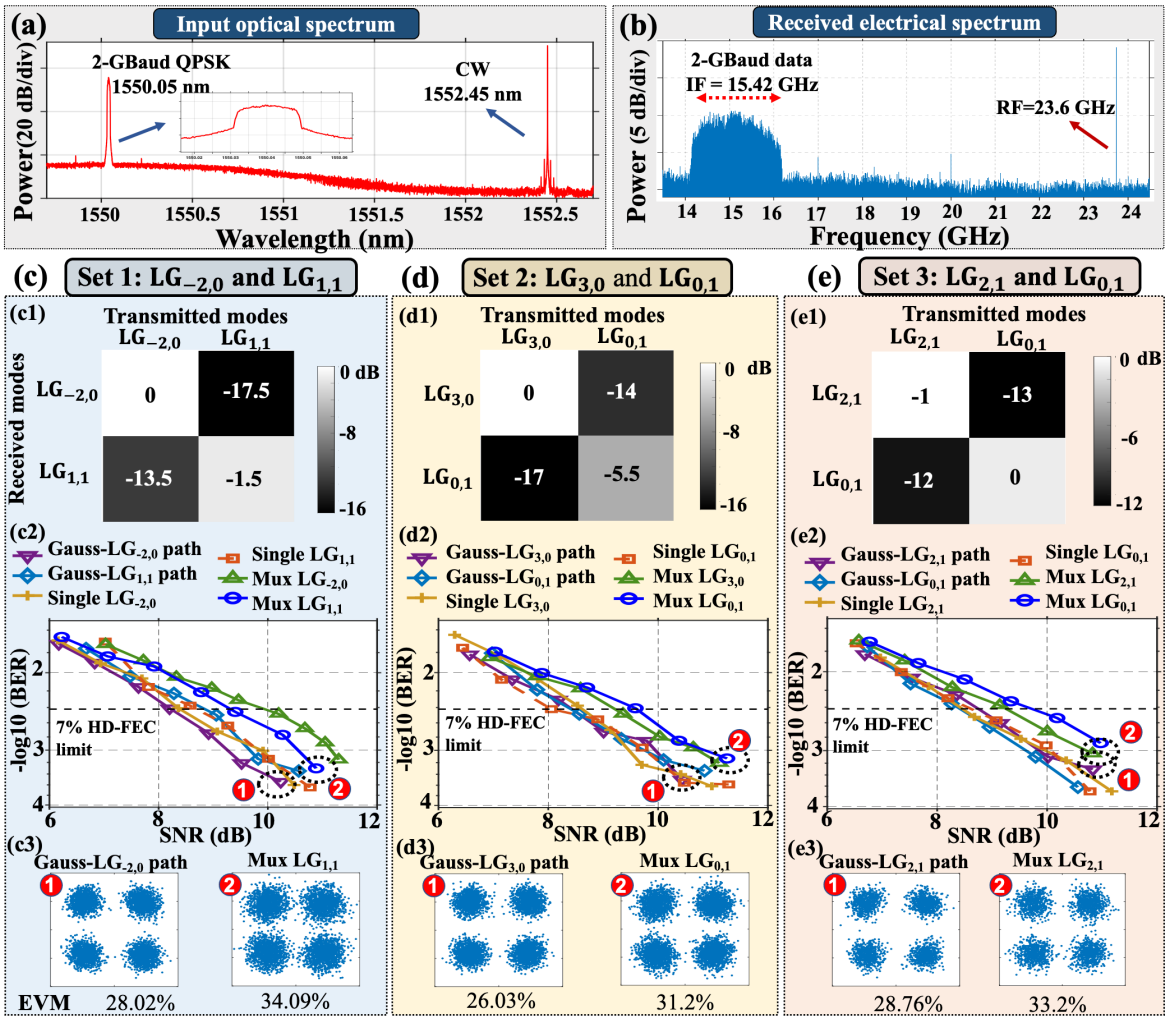

Fig. 6. (a) Input optical spectrum of 2-Gbaud QPSK data signal and CW laser source located at 1550.05 nm and 1552.45 nm, respectively. (b) Received electrical spectrum of data and RF source located at an IF frequency of 15.42 GHz and an RF frequency of 23.6 GHz, respectively. (c-e) Normalized channel crosstalk matrix in dB for Set 1 {$LG_{-2,0}$ and $LG_{1,1}$}, Set 2 {$LG_{3,0}$ and $LG_{0,1}$}, and Set 3 {$LG_{2,1}$ and $LG_{0,1}$}; the BER performance of each data channels versus the SNR when an optical power of 10.7 dBm is launched into the PIN-PD. Also shown are signal constellation diagrams at two different points with their EVM values. CW: continuous wave; IF: intermediate frequency; RF: radio frequency; BER: bit error rate; SNR: signal-to-noise ratio; EVM: error vector magnitude.

However, we measure the power coupling for few sets of modes in Fig. 6.

F. Experimental results for an LG-multiplexed THz communication link

We measure the modal crosstalk and evaluate the data transmission performance of an LG-multiplexed THz communication link in Fig. 6. The 2-Gbaud QPSK signal and a CW laser source are launched into the PIN-PD for the heterodyne photomixing process. The measured optical spectrum is shown in Fig. 6(a). The spectrum is obtained using an optical spectrum analyzer (OSA). The generation of a 0.3 THz beam corresponds to the optical wavelength difference of ~ 2.4 nm. Figure 6(b) shows the received THz electrical spectrum evaluated by the coherent receiver. The small deviation (i.e., 1.4 GHz) of IF at 15.42 GHz compared to the desired value (i.e., $f_{0.3\,THz} - 12.\, f_{RF}$) might be due to frequency drifts of the optical laser sources and the stability of the RF frequency source.

Figs. 6(c-e) show the evaluation of the 2-Gbaud QPSK signal transmission for each THz LG mode. The three different sets of modes used for multiplexing are as follows: Set 1, {$LG_{-2,0}$, $LG_{1,1}$}; Set 2, {$LG_{3,0}$, $LG_{0,1}$}; and Set 3, {$LG_{2,1}$, $LG_{0,1}$}. The first row in the figure shows the crosstalk matrices for these sets. These values are normalized received IF power when (a) two optical CW laser sources are combined and launched into the PIN-PD; (b) the input optical power to the PIN-PD is 10.7 dBm; (c) the generation and down-conversion PPs are used to generate and detect the THz LG beams; and (d) the link distance is ~ 40 cm. The modal coupling and crosstalk between the two chosen modes is < -12-dB. Specifically, the crosstalk from $LG_{2,1}$ to $LG_{0,1}$ (-12 dB) is 5-dB higher than the crosstalk from $LG_{3,0}$ to $LG_{0,1}$ (-17 dB). This increase in the modal coupling and crosstalk for higher-order LG modes might be because of (a) the transmitter/receiver misalignments and (b) the larger beam size of LG modes with higher modal indices and the subsequent beam truncation by the limited-sized receiver aperture [41-43].

To provide a larger number of channels/beams in sub-THz wireless communications using MDM of LG beams, theoretically smaller channel mode spacing (e.g., adjacent modes) between LG modes is preferred. However, in practice due to the system misalignments and imperfect components the LG modes with smaller modal spacing tends to have higher crosstalk [42-43, 45]. We have experimentally measured >-10 dB intermodal crosstalk between two adjacent modes of {$LG_{1,0}$, $LG_{1,1}$} for multiplexing, which is larger than Set 1 (i.e., {$LG_{-2,0}$, $LG_{1,1}$}). Such higher crosstalk could potentially be reduced by improving the tracking and pointing system for alignments and LG (de)multiplexers with lower modal conversion loss and crosstalk [4, 45, 47].

The dependence of BER performance with respect to the SNR is shown in Figs. 6(c-e). For each of the two paths in the setup, three cases of transmission are considered: (1) single Gaussian, (2) single LG mode, and (3) multiplexed LG modes. For simplicity, instead of using PPs based on complex-amplitude modulation to generate LG beams ($p \neq 0$), SPPs are used to generate OAM beams in a direct path, and a blazed grating is placed in the angled path of the setup to generate Gaussian beams. All channels appear to have BERs below 3.8×10^{-3} (i.e., the FEC limit [46]). Compared to a Gaussian beam transmission, multiplexed LG modes suffer from a higher SNR penalty (e.g., ~ 0.5 for Set 1 and 2, ~ 1 dB for Set 3). This penalty might originate from (a) the conversion efficiency of the generation and down-conversion approaches [32-33]; (b) the fact that the emitted beam at the output of the PIN-PD is not a pure Gaussian beam; and (c) the higher divergence and modal coupling of the higher-order LG modes (e.g., $LG_{2,1}$) [41-43].

Two examples of constellation diagrams with their corresponding error vector magnitudes (EVMs) are shown in the last row of Figs. 6(c–e). The EVM values are ~25% for the Gaussian modes and ~35% for the multiplexed LG modes at an optical power of ~10.7-dBm. The distortion of constellation diagrams and higher EVM values for multiplexed LG modes can be due to the increase in modal power coupling and higher power loss compared to those of Gaussian modes at the same SNR level.

It is worth noting that implementation and performance of MDM in sub-THz frequencies have some differences compared to optical frequencies despite their similar concept. In terms of performance, MDM system in sub-THz frequencies: (i) experiences relatively higher divergences, (ii) has smaller available spectrum for communication, and (iii) suffer less by the atmospheric turbulence and weather conditions [5-6, 8, 20]. In terms of implementation, in this experiment THz waves are generated by beating two laser sources in a PIN-PD using the heterodyning approach, wherein one of the laser sources is modulated to carry data streams. In optical frequencies, the data channels are commonly generated by modulating a single optical carrier using an amplitude/phase modulator [7-11].

We note that our demonstration is for a ~ 40 cm link distance. When transmitting longer wireless distances, LG beams will experience higher divergence and more beam truncations induced by a limited-size receiver aperture. This can increase the power coupling to neighboring LG modes with different ℓ and p indices [41-43]. For instance, we simulate a sub-THz link (e.g., 0.3 THz) while transmitting an $LG_{1,1}$ mode, as shown in Table I. When increasing the beam width and receiver aperture diameter by a factor of five in the simulation model, the power loss and highest crosstalk could be reduced. However, longer link distances may be feasible to accommodate by the following: (i) higher transmission power to overcome the atmospheric attenuation [8, 46]; (ii) different diffraction patterns with higher conversion efficiencies for different LG modes [33-34], and (iii) larger transmitted beam waist and receiver aperture to address the issue of beam divergence [47].

TABLE I
SIMULATION RESULTS OF LONGER WIRELESS DISTANCES WHEN TRANSMITTING AN $LG_{1,1}$ MODE

	Link distance	**0.4 m**	**4 m**	**10 m**
Case 1 beam width 10 mm receiver aperture diameter 10 cm	**Power loss (dB)**	~ 0.4	~ 7.4	~ 13.7
	Crosstalk (dB)	~ -15	~ -8.6	~ -6.2
Case 2 beam width 50 mm receiver aperture diameter 50 cm	**Power loss (dB)**	~ 0	~ 1.6	~ 11.5
	Crosstalk (dB)	~ -28	~ -7	~ -6

III. SUMMARY

In summary, we have experimentally demonstrated THz MDM of LG beams when varying two different modal indices. By designing specific PPs, THz LG beams can be generated and detected. The proposed method can enable THz MDM in a 2D modal basis set using LG modes (i.e., both ℓ and p) instead of a 1D modal basis set using OAM modes (i.e., only ℓ). Data transmission at a total data rate of 8-Gbit/s is performed at 0.3 THz over a ~ 40-cm link for two multiplexed modes. When using higher-order LG modes varying two indices for MDM: (a) divergence, beam size, and power loss can increase; and (b) a higher modal coupling and crosstalk can occur due to link misalignment and beam truncation by the limited-sized receiver aperture.

REFERENCES

[1] H. Song and T. Nagatsuma, "Present and future of Terahertz communications," *IEEE Transactions on Terahertz Science and Technology*, vol. 1, no. 1, pp. 256-263, Sep. 2011.

[2] H. Tataria, M. Shafi, A. F. Molisch, M. Dohler, H. Sjöland, and F. Tufvesson, "6G wireless systems: vision, requirements, challenges, insights, and opportunities," *Proceedings of the IEEE*, pp. 1-34, 2021.

[3] T. Nagatsuma, G. Ducournau and C. C. Renaud, "Advances in terahertz communications accelerated by photonics," *Nat. Photon.*, vol. 10, no. 6, pp. 371-379, Jun. 2016.

[4] H. Elayan, O. Amin, B. Shihada, R. M. Shubair, and M.-S. Alouini, "Terahertz band: The last piece of RF spectrum puzzle for communication systems," *IEEE Open J. Commun. Soc.*, vol. 1, pp. 1–32, 2020.

[5] J. Ma, L. Moeller, J. F. Federici, "Experimental comparison of terahertz and infrared signaling in controlled atmospheric turbulence," *J. Infr. Millim. Terahertz Waves*., vol. 36, no. 2, pp. 130–143, 2015.

[6] Z. Zhao, R. Zhang, H. Song, K. Pang, A. Almaiman, H. Zhou, H. Song, C. Liu, N. Hu, X. Su, A. Minoofar, H. Sasaki, D. Lee, M. Tur, A. F. Molisch, and A. E. Willner, "Modal coupling and crosstalk due to turbulence and divergence on free space THz links using multiple orbital angular momentum beams," *Sci. Rep.*, vol. 11, Jan. 2021, Art. No. 2110.

[7] A. J. Seeds, H. Shams, M. J. Fice, and C. C. Renaud, "TeraHertz photonics for wireless communications," *J. Lightw. Technol.*, vol. 33, no. 3, pp. 579-587, Feb. 2015.

[8] T. Harter, C. Fullner, J. N. Kemal, S. Ummethala, J. L. Steinmann, M. Brosi, J. L. Hesler, E. Brundermann, A. -S. Muller, W. Freude, and S. Randel, "Generalized Kramers-Kronig receiver for coherent terahertz communications," *Nat. Photon.*, vol. 14, pp. 601-606, 2020.

[9] C. Castro, S. Nellen, R. Elschner, I. Sackey, R. Emmerich, T. Merkle, B. Globisch, D. de Felipe, and C. Schubert, "32 GBd 16QAM wireless transmission in the 300 GHz band using a PIN diode for THz upconversion," in *Proc. Opt. Fiber Commun. Conf.*, San Diego, CA, USA, 2019, Paper M4F.5.

[10] L. K. Oxenlewe, S. Jia, X. Pang, O. Ozolins, X. Yu, H. Hu, P. Guan, F. Da Ros, S. Popov, G. Jacobsen, M. Galili, D. Zibar, and T. Morioka, "100s gigabit/s THz communication," in *Proc. Conf. Lasers Electro-Opt*., 2018, Paper STu3D.1.

[11] H. Shams, M. J. Fice, K. Balakier, C. C. Renaud, F. van Dijk, and A. J. Seeds, "Photonic generation for multichannel THz wireless communication," *Opt. Express*, vol. 22, no. 19, pp. 23465-23472, Sep. 2014.

[12] D. J. Richardson, J. M. Fini, and L. E. Nelson, "Space-division multiplexing in optical fibres," *Nat. Photon.*, vol. 7, no. 5, pp. 354-362, 2013.

[13] G. Li, N. Bai, N. Zhao, and C. Xia, "Space-division multiplexing: the next frontier in optical communication," *Adv. Opt. Photon.*, vol. 6, no. 4, pp. 413-487, 2014.

[14] H. Zhang *et al*., "Tbit/s Multi-Dimensional Multiplexing THz-Over-Fiber for 6G Wireless Communication," *J. Lightw. Technol.*, vol. 39, no. 18, pp. 5783-5790, Sep. 2021.

[15] V. S. Pavelyey, K. N. Tukmakov, Yu. Yu. Choporova, N. D. Osintseva, and B. A. Knyazev, "Towards multichannel terahertz telecommunication based on mode division multiplexing," AIP Conference Proceedings 2299, 030002, 2020.

[16] A. M. Yao and M. J. Padgett, "Orbital angular momentum: origins, behavior and applications", *Adv. Opt. Photon.*, vol. 3, pp. 161-204, 2011.

[17] L. Allen, M. W. Beijersbergen, R. J. C. Spreeuw, and J. P. Woerdman, "Orbital angular momentum of light and the transformation of Laguerre-Gaussian laser modes", *Phys. Rev. A.*, vol. 45, pp. 8185-8189, 1992.

[18] G. Gibson, J. Courtial, M. J. Padgett, M. Vasnetsov, V. Pas'ko, S. M. Barnett, and S. Franke-Arnold, "Free-space information transfer using light beams carrying orbital angular momentum," *Opt. Express*, vol. 12, no. 22, pp. 5448-5456, Nov. 2004.

[19] R. M. Henderson, "Let's do the twist!: radiators, experiments, and techniques to generate twisted waves at radio frequencies," *IEEE Microwave Magazine*, vol. 18, no. 4, pp. 88-96, Jun. 2017.

[20] S. Koenig, D. Lopez-Diaz, J. Antes, F. Boes, R. Henneberger, A. Leuther, A. Tessmann, R. Schmogrow, D. Hillerkuss, R. Palmer, T. Zwick, C. Koos, W. Freude, O. Ambacher, J. Leuthold, and I. Kallfass, "Wireless sub-THz communication system with high data rate," *Nat. Photon.*, vol. 7, pp. 977–981, Oct. 2013.

[21] X. Li, J. Yu, K. Wang, M. Kong, W. Zhou, Zihang Zhu, C. Wang, M. Zhao, and G-K. Chang, "120 Gb/s wireless terahertz-wave signal delivery by 375 GHz-500 GHz multi-carrier in a 2 × 2 MIMO system," *J. Lightw. Technol.*, vol. 37, no. 2, pp. 606-611, Jan. 2019.

[22] S. Jia, L. Zhang, S. Wang, W. Li, M. Qiao, Z. Lu, N. M. Idrees, X. Pang, H. Hu, X. Zhang, L. K. Oxenløwe, and X. Yu, "2 × 300 Gbit/s line rate PS-64QAM-OFDM THz photonic-wireless transmission," *J. Lightw. Technol.*, vol. 38, no. 17, pp. 4715-4721, Sep. 2020.

[23] X. Su, H. Zhou, K. Zou, A. Minoofar, H. Song, R. Zhang, K. Pang, H. Song, N. Hu, Z. Zhao, A. Almaiman, S. Zach, M. Tur, A. F. Molisch, H. Sasaki, D. Lee, and A. E. Willner, "Demonstration of 8-Channel 32-Gbit/s QPSK wireless communications at 0.28-0.33 THz using 2 frequency, 2 polarization, and 2 mode multiplexing," in *Proc. Opt. Fiber Commun. Conf.*, San Francisco, CA, USA, 2021, Paper M3J.4.

[24] A. Trichili, C. Rosales-Guzman, A. Dudley, B. Ndagagno, A. Ben Salem, M. Zghal, and A. Forbes, "Optical communication beyond orbital angular momentum," *Sci. Rep.*, vol. 6, Jun. 2016, Art. No. 27674.

[25] G. Xie, Y. Ren, Yan Yan, H. Huang, N. Ahmed, L. Li, Z. Zhao, C. Bao, M. Tur, S. Ashrafi, and A. E. Willner, "Experimental demonstration of a 200-Gbit/s free-space optical link by multiplexing Laguerre–Gaussian beams with different radial indices," *Opt. Lett.*, vol. 41, no. 15, pp. 3447-3450, 2016.

[26] Y. Hira and Y. Monnai, "Sub-terahertz vortex beam generation using a spiral metal reflector," *Opt. Express*, vol. 29, no. 15, pp. 24118-24128, 2021.

[27] J. He, X. Wang, D. Hu, J. Ye, S. Feng, Q. Kan, and Y. Zhang, "Generation and evolution of the terahertz vortex beam," *Opt. Express*, vol. 21, no. 17, pp. 20230-20239, 2013.

[28] K. Cheng, Z. Hu, Y. Wang, J. Ma, and J. Wang, "High-performance terahertz vortex beam generator based on square-split-ring metasurfaces," *Opt. Lett*., vol. 45, no. 21, pp. 6054-6057, 2020.

[29] K. Miyamoto, K. Sano, T. Miyakawa, H. Niinomi, K. Toyoda, A. Vallés, and T. Omatsu, "Generation of high-quality terahertz OAM mode based on soft-aperture difference frequency generation," *Opt. Express*, vol. 27, no. 22, pp. 31840-31849, 2019.

[30] H. Zhou, X. Su, A. Minoofar, R. Zhang, H. Song, K. Pang, K. Zou, H. Song, N. Hu, Z. Zhao, A. Almaiman, S. Zach, M. Tur, A. F. Molisch, H. Sasaki, D. Lee, and A. E. Willner, "Experimental demonstration of 8-Gbit/s QPSK communications using two multiplexed orbital-angular-momentum beams in the 0.27-0.33 THz range," in *Proc. Conf. Lasers Electro-Opt.*, 2021, Paper STh2F.7.

[31] A. Minoofar, X. Su, H. Zhou, F. Alishahi, K. Pang, K. Zou, R. Zhang, S. Zach, M. Tur, A. F. Molisch, H. Sasaki, D. Lee, and A. E. Willner, "Experimental demonstration of free-space sub-THz communications link using multiplexing of beams having two different LG modal indices," in *Proc. Eur. Conf. Opt. Commun.*, Bordeaux, France, 2021, Paper Th2B.3.

[32] T. Ando, Y. Ohtake, N. Matsumoto, T. Inoue, and N. Fukuchi, "Mode purities of Laguerre-Gaussian beams generated via complex-amplitude modulation using phase-only spatial light modulators," *Opt. Lett.*, vol. 34, no. 1, pp. 34-36, 2009.

[33] J. Arlt, K. Dholakia, L. Allen, and M. Padgett, "The production of multiringed Laguerre–Gaussian modes by computer generated holograms," *J. Mod. Opt.*, vol. 45, no. 6, pp. 1231-1237, 1998.

[34] J. Leach, M. R. Dennis, J. Courtial, and M. J. Padgett, "Vortex knots in light," *New J. Phys*., vol. 7, no. 55, pp. 1-11, 2005.

[35] E. Bolduc, N. Bent, E. Santamato, E. Karimi, and R. W. Boyd, "Exact solution to simultaneous intensity and phase encryption with a single phase-only hologram," *Opt. Lett.*, vol. 38, no. 18, pp. 3546-3549, 2013.

[36] A. Siemion, "The magic of optics-An overview of recent advanced Terahertz diffractive optical elements," *Sensors*, vol. 21, no. 1, 2020.

[37] L. Liebermeister, S. Nellen, R. B. Kohlhaas, S. Lauck, M. Deumer, S. Breuer, M. Schell, and B. Globisch, "Optoelectronic frequency-modulated continuous-wave terahertz spectroscopy with 4 THz bandwidth," Nature Communications, vol. 12, no. 1, pp. 1-10, 2021.

[38] J. Smith, M. Naftaly, S. Nellen, and B. Globisch, "Beam profile characterisation of an optoelectronic silicon lens-integrated pin-pd emitter between 100 ghz and 1 thz," *Appl. Sci.*, vol. 11, no. 2, pp. 1-12, 2021.

[39] S. Restuccia, Daniel Giovannini, Graham Gibson, and M. Padgett, "Comparing the information capacity of Laguerre–Gaussian and Hermite–Gaussian modal sets in a finite-aperture system," *Opt. Express*, vol. 24, no. 24, pp. 27127-27136, 2016.

[40] A. D'Errico, R. D'Amelio, B. Piccirillo, F. Cardano, and L. Marrucci, "Measuring the complex orbital angular momentum spectrum and spatial mode decomposition of structured light beams," *Optica*, vol. 4, no. 11, pp. 1350–1357, 2017.

[41] R. L. Phillips and L. C. Andrews, "Spot size and divergence for Laguerre Gaussian beams of any order," *Appl. Opt.*, vol. 22, no. 5, pp. 643-644, 1983.

[42] Z. Mei, and D. Zhao, "The generalized beam propagation factor of truncated standard and elegant Laguerre-Gaussian beams," *J. Opt. A: Pure Appl. Opt.*, vol. 6, no. 11, pp. 1005–1011, 2004.

[43] X. Zhong, Y. Zhao, G. Ren, S. He, and Z. Wu, "Influence of finite apertures on orthogonality and completeness of Laguerre-Gaussian beams," *IEEE Access*, vol. 6, pp. 8742–8754, Feb. 2018.

[44] P. Girshovitz and N. T. Shaked, "Real-time quantitative phase reconstruction in off-axis digital holography using multiplexing," *Opt. Lett.*, vol. 39, no. 8, pp. 2262–2265, Apr. 2014.

[45] G. Xie et al., "Performance metrics and design considerations for a free-space optical orbital-angular-momentum-multiplexed communication link," *Optica*, vol. 2, no. 4, p. 357, Apr. 2015.

[46] F. Chang, K. Onohara, and T. Mizuochi, "Forward error correction for 100G transport networks," *IEEE Commun. Mag.*, vol. 10, no. 3, pp. S48–S55, Mar. 2010.

[47] C. Chaccour, M. N. Soorki, W. Saad, M. Bennis, P. Popovski, and M. Debbah, "Seven defining features of terahertz (THz) wireless systems: A fellowship of communication and sensing," *IEEE Communications Surveys & Tutorials*, 2022.

[48] N. T. Yardimci, S.-H. Yang, C. W. Berry, and M. Jarrahi, "High-power terahertz generation using large-area plasmonic photoconductive emitters," *IEEE Trans. THz Sci. and Technol.*, vol. 5, no. 2, pp. 223-229, Mar. 2015.

[49] Y. Yagi, H. Sasaki, T. Semoto, T. Kageyama, T. Yamada, J. Mashino, D. Lee, "Field Experiment of 117 Gbit/s wireless transmission using OAM multiplexing at a distance of 200 m on 40 GHz band," in *Proc. IEEE International Conf. on Commun. Workshops (ICC Workshops)*, pp. 1-5, 2021.